



Energy Management Strategy for Multi-Source Electric Vehicles

Anbarasan C¹, R.Nagarajan² and S.Kannadhasan³¹ Department of Electrical and Electronics Engineering, Gnanamani College of Technology, Namakkal, Tamilnadu, India and,² Department of Electrical and Electronics Engineering, Gnanamani College of Technology, Namakkal, Tamilnadu, India and³ Department of Electronics and Communication Engineering, Study World College of Engineering, Coimbatore, Tamilnadu, India.

ARTICLE INFO

Article history:

Received: 10 February 2023;

Received in revised form:

15 March 2023;

Accepted: 25 March 2023;

Keywords

Energy,

PSO,

Electric Vehicle,

Optimization.

ABSTRACT

This project proposes a real time fuzzy assisted particle swarm optimization (PSO) based energy management strategy for the multi-source electric vehicles (EVs). In pure EVs the major on-board energy source is the battery which is generally accompanied with other sources such as fuel cell (FC), ultra capacitor (UC) to improve its life time. The energy management algorithm which is formulated as an optimization problem in this project provides optimum sharing of energy sources to meet the vehicle load requirement at every instant without any prior knowledge about the driving profile. The proposed algorithm is simple, efficient and can be easily implemented in a low cost embedded system.

© 2023 Elixir All rights reserved.

1. Introduction

The development of modern societies is closely linked to people and goods mobility. However, economic, ecological and geopolitical aspects related with energy availability impose difficult challenges to achieve sustainable mobility. Due to its very high efficiency and much smaller local/global emission levels comparatively to internal combustion engines vehicles, electric traction has a fundamental place in sustainable mobility, especially road electric vehicles (EVs). Nevertheless, EVs still have a major drawback: energy storage. For massive deployment of EVs the driving range, charging time and lifetime problems must be solved. Typically, an EV stores energy in batteries that are bulky, heavy and expensive. Due to this problem, with current battery technology, it is very difficult to make a general purpose EV that effectively competes with ICE cars. At present and in the foreseeable future, the viable EV energy sources are batteries, fuel cells, SuperCapacitors (SCs) and ultra-high speed flywheels. Batteries are the most mature source for EV application but currently they offer either high specific energy (HSE) or high specific power (HSP). Fuel cells are expensive and less mature for EV application. They can offer exceptionally HSE, but with very low specific power [1]-[5]. Such low specific power almost rules out their standalone application in EVs that require a high acceleration rate or hill climbing capability, and they are incapable of accepting the regenerative energy during EV braking or downhill driving. Presently, available SCs do not have the energy capacity needed for standalone application. However, SCs can offer exceptionally HSP and thus be used in several applications for energy storage and management. The SCs main application is to limit the power restrictions on energy sources such as batteries or fuel cells. Flywheels are currently technologically immature for EV application. Full EV solutions require significant progresses in battery technology and/or also using

different energy sources with optimized management of the energy flow, which is the subject of this work.

As in current EVs, in full electric hybridized EVs batteries are the main source and therefore the overall objective should be based on the maximization of SoC, leading to the use of the SCs to respond to peak power demand during traction operation and store the maximum amount of energy from vehicle deceleration and braking. This requires that, at each instant, the SCs have the SoC level to help the batteries in the traction mode within the vehicle performance limits, as well as to absorb most of the energy produced by the motor during braking mode. Therefore, this planning strategy should define a scheme to keep the SCs' SoC at an appropriate level for any request. From these analyses, one can derive the impact of the working temperature on the battery performances over its lifetime. At elevated temperature (40°C), the performances are less compared to at 25°C [6]-[10]. The obtained mathematical expression of the cycle life as function of the operating temperature reveals that the well-known Arrhenius law cannot be applied to derive the battery lifetime from one temperature to another. Moreover, a number of cycle life tests have been performed to illustrate the long-term capabilities of the proposed battery cells at different discharge constant current rates. The results reveal the harmful impact of high current rates on battery characteristics. On the other hand, the cycle Lithium ion batteries offer an attractive solution for powering electric vehicles due to their relatively high specific energy and specific power, however, the temperature of the batteries greatly affects their performance as well as cycle life.

In this work, an empirical equation characterizing the battery's electrical behavior is coupled with a lumped thermal model to analyze the electrical and thermal behavior of the 18650 Lithium Iron Phosphate cell. Under constant current discharging mode, the cell temperature increases with

increasing charge/discharge rates. The dynamic behavior of the battery is also analyzed under a Simplified Federal Urban Driving Schedule and it is found that heat generated from the battery during this cycle is negligible. Simulation results are validated with experimental data. The validated single cell model is then extended to study the dynamic behavior of an electric vehicle battery pack. The modeling results predict that more heat is generated on an aggressive US06 driving cycle as compared to UDDS and HWFET cycle. An extensive thermal management system is needed for the electric vehicle battery pack especially during aggressive driving conditions to ensure that the cells are maintained within the desirable operating limits and temperature uniformity is achieved between the cells.

Based on the porous electrode and concentrated solution theory, a thermal model is developed for lithium ion battery pack. The accuracy of predicted battery temperatures is validated by charge–discharge cycling experiments under natural and forced convection conditions. The heat generation and dissipation rates of battery under different conditions are simulated by the proposed model and the results indicate that: (1) the SOC change has a significant effect on the reversible heat generation rate but has almost no influence on the irreversible heat generation rate; (2) the generation rates of reversible and irreversible heat during charge are almost equal to that during discharge with the same SOC and current rate, but the effect of reversible heat on battery temperature is opposite; (3) for enhancing heat dissipation with a given input power of cooling fan, there always exists an optimum value for the resistance coefficient of battery pack, and the optimal coefficient is increased when the input power of fan increases. In addition, the comparisons between the predicted and measured battery temperature indicate that, the reversible heat has significant influence on battery temperature during continuous charge and discharge, especially under low current rate, but the influence can't be observed during charge–discharge cycles [11]-[15].

2. Related Work

The decomposition of management and control in different levels has been proposed in others approaches, such as Energetic Macroscopic Representation (EMR) and multi-level control scheme. In a maximum control structure is then derived from the EMR of the storage system. Also in a unified control structure suitable for different HEVs is introduced and derived from a global model using EMR by the inversion-based control principle. In the authors also discussed how energy management of different hybrid vehicles could be achieved in a general way, while hybrid vehicles can be very different from each other. In this work, the multi-source EV management scheme to be implemented as an online process focuses on the overall system with different time scales and three subsystems or levels may be identified. The long-term is related to the energy management strategy, the short-term actuation planning is linked to the power management strategy, and the very short-term is associated with the power electronic converters operation and their dynamics. In Fig. 1 the hierarchy structure of the subsystems that compose the Multi-level EMS is presented.

The overall multi-source EV energy management problem for the dual hybrid energy source constituted by batteries and SCs, presented in Fig. 1.1, consists in minimizing the difference between the power demand and the power supplied by the sources, while keeping the battery and SCs SoC at their optimal value. The power management problem consists in instantaneously determining the power share between the two

sources while regulating the DC link voltage. These two problems cannot be completely decoupled and should be jointly tackled.

To achieve this goal, there are two fundamental sub-problems that must be addressed. Firstly, at the energy management level, we should provide guidance for the correct operating range of the batteries and SCs as a function of power system requests. Secondly, at the power management level, we must decide how to split the requested power between batteries and SCs [16]-[24].

Globally, the main objective of the energy management involves establishing the operation range of the sources in the better position to respond to the power requests subject to constraints defined by the efficient limits of the sources' SoC. For the power management, the fundamental objective is continuously feeding the powertrain requests with the available energy in the sources (Eq. (2.1.3)), while satisfying the maximum power of the batteries and SCs constraints, which are updated at each iteration of the algorithm (Eq. (2.1.2)).

The energy management system is decomposed into three levels (strategy, tactical and operational). The first two levels are introduced and fully explained in this paper. The EMS is based on long-term (energy) and a short-term (power) management. The long-term (with a decision refresh of 1 s) is developed using a dynamic restricted search space using a set of rules, that result of the energy sources' SoC mapping into a search space (see Fig. 2). The short-term (with a decision refresh of 10 ms) is implemented by an optimization strategy (Simulated Annealing technique).

3. Proposed System

In a first step, a study of the energy and power management implies a definition of energy source models. Although more precise models for the SC and batteries are available, we consider that, for the purpose of this work, simplified energy source models are adequate to compute optimal power sharing without introducing unnecessary complexity. Thus, the state of charge (SoC_i) and the charge (Q_i) in the SCs and battery can be calculated by (1):

$$SoC_i(t) = \frac{Q_i(t)}{Q_{iRef}}, i = \{bat, SC\} \quad (1)$$

where Q_{iRef} is the nominal capacity of the energy source. The simplified equivalent model for a SC consists of an ideal capacitor in series with a very small value resistor, and the simplified battery model is represented by a variable DC source and a small value resistor. The voltage values of the capacitor and the DC source depend on their SoC and the resistors values are a function of the sources degradation. Considering that the battery open-circuit voltage has a linear dependence on SoC_i(t), then both open-circuit voltages are given by (2):

$$v_i^{OC}(t) = V_i^{OC,min} + \delta_i \cdot SoC_i(t), i = \{bat, SC\} \quad (2)$$

where $V_i^{OC,min}$ is the minimum open-circuit voltage and δ_i is the SoC_i gain. Particularizing for our problem, the objective function presented in (4.1.4) is developed in (4.1.7).

$$f_o = \min_{C_{bat}, C_{SC}} |P_{dem}[k] - [C_{bat}[k] \cdot P_{bat}^{max}[k] + C_{SC}[k] \cdot P_{SC}^{max}[k]|, \quad (3)$$

$$\forall k \in \{1, \dots, N\} \quad \text{--- 4.1.7}$$

Subject to:

$$C_i \in [LB_i, UB_i] \\ P_i[k] = C_i[k] \cdot P_i^{max}[k]$$

$$\begin{aligned}
SoC_i[k] &= \frac{Q_i[k]}{Q_{iRef}} \\
v_i^{OC}[k] &= V_i^{OC.min} + \delta_i \cdot SoC_i[k] \\
I_i[k] &= \frac{P_i[k]}{v_i^{OC}[k]} \\
Q_i[k+1] &= Q_i[k] - I_i[k] \cdot \frac{\Delta t}{3600} \\
P_i^{max}[k+1] &= v_i^{OC}[k] \cdot I_{iRef} \\
P_{i.min} &\leq P_i[k] \leq P_{i.max} \\
SoC_i^{min} &\leq \frac{Q_i[k]}{Q_{iRef}} \leq SoC_i^{max}
\end{aligned}$$

With $i \in \{bat, SC\}$ and $k \in \{1, \dots, N\}$.

Two types of constraints may be considered. The first type (equality constraints) defines the technical evolution of the source parameters (power, voltage and current) and the second type (inequality constraints) is the SoC operation range, which is directly affected by the source parameters evolution. Basically, if the battery and SCs SoC is too high then the ability to recuperate braking energy decreases, which results in the waste of the surplus energy. Conversely, if the SoC is too low then energy sources may not supply enough power to meet the EV requirements when accelerating. In order to extend the battery and SCs lifecycle, their SoC should operate in a proper range as much as possible:

$$SoC_i^{min} \leq \frac{Q_i[k]}{Q_{iRef}} \leq SoC_i^{max} \quad (4)$$

A high management level for the global EMS is designed to dynamically limit the solution space search according to P_{dem} and the SoCs.

The high level management strategy is defined based on a set of rules, determined mainly by experience and expert knowledge, based on (2.1.3), using the values of the SoC for battery and SCs, $SoC_i(t)$, and the power demand of the supply system, $P_{dem}(t)$, at every instant, t . Accordingly, in every decision of this management level, with a periodicity 1 s, the search space is restricted by imposing a lower bound, LB_i , and an upper bound, UB_i , in $C_i(t)$, i.e., $C_i(t) \in [LB_i, UB_i]$, with $LB_i \geq LB_i^{max}$ and $UB_i \geq UB_i^{max}$, to subsequently obtain an optimal solution to $C_i(t)$. This is presented in Fig. 3.2. The strategy is based on the SoC map of the two sources, where thresholds have been defined for ensuring a correct operation. The search space is restricted as a function of SoC status and helps the optimization method to find a better solution quickly, by narrowing the scope of the search to the regions of interest. The use of thresholds provides anticipation capacity to this level, positioning the SoC (especially for SCs) at levels that may help the EV in subsequent operations.

Considering a simple displacement of a vehicle, there is a standing phase (stopped vehicle), an acceleration phase (light or high acceleration), a phase of constant speed operation (cruising) and a deceleration phase (or breaking). From this operation decomposition, the energy trading priorities needed to respond to the driver requests can be defined, using the energy sources previously selected. So, three types of rules are defined to sustain the long term strategy planning:

- Weak rules (Fig. 3): Set of rules 1 (SR1): Standing; SR2: Light Accelerating or Cruising;
- Medium rules (Fig. 4): SR3: High Acceleration; SR4: Decelerating or Breaking; and
- Strong rules (Fig. 5): SR5: Minimum values of SoC_i ; SR6: Maximum values of $S C_i$.

The sets of rules are implemented with if-then operation rules as a function of P_{dem} and SoC_i using thresholds defined

by a fine-tuning process with a complete knowledge of the characteristics and efficiency of the sources used. These rules are applied sequentially, testing each subgroup, from the most to the less dominant one (strong to weak rules). A flowchart of the dynamic search space restriction process is presented in Fig. 4.4. The strong rules correspond to extreme situations such as when the SoC_{bat} and SoC_{SC} levels are below their lower bound leading to stop the EV operation, with the impossibility of providing energy from any source because the solution space for C_i becomes empty.

In order to understand the underlying rationale and the operation mode of these rules take, for example, the Set of rules 1: Standing, a weak rule set presented in Fig. 3. Responding to the power requirement (P_{dem}) and to the state of charge of both batteries and SCs (SoC_{bat} and SoC_{SC} , i.e. the ‘‘SoC map’’ presented on the left hand side of Fig. 3.2), the rules generate the constraint ‘‘Search Space’’, presented on the right hand side of Fig. 3, to be later used by the lower level power management. So, if $P_{dem}(t) = 0$ and the SoC_{bat} and SoC_{SC} levels are high (see region A in SoC map graph of Fig. 3), then the search space is reduced to $C_i \in [0, 0]$ (see Space A in Search space graph of Fig. 3). This means that if there is no power requested and both the batteries and the SCs are well charged, nothing is supposed to happen. On the other hand, if $P_{dem}(t) = 0$ and SoC_{SC} is low (below a $\tau_{SoC_{SC}}^{min}$ threshold) and the batteries still have enough energy (above a $\tau_{SoC_{bat}}^{min}$ threshold, region B in SoC map graph of Fig. 3), the search space is defined to $C_{bat} \in [0, 1]$ and $C_{SC} \in [-1, 0]$ (Space B in Search space graph of Fig. 3), i.e. the batteries will charge the SCs in order to enable future accelerations requiring a power peak to be supplied by SCs. Inversely, when the SoC_{SC} has a very high value (see region C in SoC map graph of Fig. 3) and also $P_{dem}(t) = 0$, the search space is restricted to $C_{bat} \in [-LB_{bat}^{max}, 0]$ and $C_{SC} \in [0, 1]$ (Space C in Search space graph of Fig. 3), i.e. the SCs discharge to the batteries for leveling the SoC_{SC} to a value allowing to store in the SCs the energy that can result from future EV braking. For the other weak (SR2), medium (SR3 and SR4) and strong rules (SR5 and SR6) the same approach is applied and the corresponding sets of rules are presented in Figs. 3 and 3.

The primary objective of the power management level is continuously feeding the powertrain request with the available energy. The (short-term) power management has to define an online energy sharing under the strict guidelines of strategy planning based on the long-term rules presented above. This short-term planning aims at producing a set of decisions for a high performance energy usage for any journey. To supply the power requested by the EV without interruption and degradation of the sources and the EV operation, the power management level decisions should be made within the operating space constraints defined by the energy management level according to the drivers’ requests. Therefore, the power management level defines the reference levels to control the operational level using the power reference signals. This is accomplished by transferring the response to high peak powers to the SCs, avoiding source overloading in the discharge and charge processes and preventing high frequency battery power fluctuations. The expected results are fundamentally the batteries efficiency improvement, higher life cycle and operating range increase. This level has been implemented using a SA-based approach to obtain an optimized online energy sharing between sources.

SA to deal with complex optimization problems was initially proposed by Kirkpatrick et al., based on the Metropolis algorithm, to solve combinatorial problems

although it is also effective to tackle continuous optimization problems. An analogy is established between the thermodynamic simulation parameters and those in local optimization methods. Basically, SA establishes a correspondence between the molecular process in which each molecule is positioned in different energy states looking for equilibrium, and the solution “visited” through a local search method. This molecular distribution adopts the Boltzmann criterion in which each movement will be accepted if the system energy decreases or with a proportional Boltzmann’s probability otherwise. Such probabilities are based on the annealing process and they are obtained as a function of the system temperature. In order to obtain a high probability to accept non-improving movements, the SA strategy starts with a high initial temperature. With the progress towards the optimal solution, the temperature and consequently the probability to accept a worst solution decreases. The most important parameters are the annealing temperature (T), the number of iterations at constant temperature (N) and the temperature reduction coefficient (α), which require to be tuned for obtaining good results. An SA pseudo-code is presented in Appendix A, which has been implemented in MATLAB.

The initial solution considered in our experiments has $C_{bat}[k] = C_{SC}[k] = 0$. Depending on the SoC of each source the energy management level reduces the search space by directing the algorithm to the quadrant of interest (Figs. 4). The stopping criterion considers the overall performance in recent iterations: if there are no new occurrences of a better solution for a predefined number of consecutive iterations, it is assumed that the method converged and the incumbent solution is retained. SA computes the optimal power assignment factors, $C_i[k]$, of each source to minimize the gap between the power demand, P_{dem} , and the feeding powers, P_i , at each time interval, k ,

Several simulations were carried out for some typical driving cycles (ECE, NEDC, ARTEMIS, FTP75 and NYCC) to assess the performance of the proposed online multi-source EV EMS. Driving cycles are defined as the test cycles applied to standardize the evaluation of the vehicle fuel economy and emissions. Driving cycles are speed-time sequences that represent the traffic conditions and driving behavior in a specific area. In this paper results of the ECE 15 and ARTEMIS Low Motor Urban Total are provided. The EV used in the experiments is the result of the VEIL project (“Veículo Eléctrico Isento de Licença de condução”, meaning License Free Electric Vehicle) based on the GL 162 Ligier small urban vehicle. Based on the information of the ECE 15 and ARTEMIS vehicle speed profile (upper graphics of Fig. 5), on $v_{cycle}(t), t \in [0, T]$ and the VEIL project vehicle characteristics, given in Table 5.1, the mechanical power, $P_{mec_{cycle}}(t), t \in [0, T]$, at the vehicle wheel is computed.

Table 5.1 VEIL Project Vehicle Specifications

Parameter	Value
Vehicle mass (kg)	500
Rolling resistance coefficient	0.015
Aerodynamic drag coefficient	0.51
Front area (m ²)	2.4
Wheels radius (m)	0.26
Gearbox transmission ratio	10

In previous VEIL project works, the global system efficiency of the vehicle, considering the efficiencies of the electric motor (η_m), inverter (η_{VFD}) and DC/DC converter (η_{Conv}) as a function of the vehicle speed, was measured and

registered for several on-road tests. Fig. 7 presents the VEIL powertrain efficiencies.

The efficiency values are applied to the $P_{mec_{cycle}}(t)$ in order to compute the electrical power demand, $P_{mec_{cycle}}(t), t \in [0, T]$, requested from the energy sources, as presented in (5.3).

$$P_{dem}(t) = \frac{P_{mec_{cycle}}(t)}{\eta_m(t) \cdot \eta_{VFD}(t) \cdot \eta_{Conv}(t)} \quad (5)$$

The VEIL electrical power demand is then presented in the lower graphics of Fig. 5.1 (a) and (b).

The next vehicle operation is acceleration where the two sources are required to feed the vehicle powertrain. Now the strategy level leads the SA algorithm to the search space referred as CASE G in Fig. 4.2. During the subsequent displacement at constant speed, the required power is below the batteries maximum power and the SCs’ SoC is still below its minimum threshold. Therefore, the strategy level restricts the search space for the SA algorithm to the region indicated as CASE E in Fig. 6, where the solutions means that batteries are feeding the powertrain and charging the SCs. The following phase is the vehicle deceleration and the SCs’ SoC is still low; the strategy level restricts the search space to a region referred as CASE I in Fig. 6. In this state, all the regenerative braking energy is stored in SCs and also some energy is transferred from the batteries to the SCs.

The previous description is repeated in the next vehicle displacement since the SCs do not have recovered a SoC level of at least 80%. Thus, up to 106 s, the strategy level guides the SA algorithm to the same search spaces when the vehicle has the same operation conditions. At this moment, the SCs’ SoC value is over its minimum threshold and the batteries SoC is within the allowed range and $P_{dem} = 0$; then the strategy level guides the SA algorithm to the search space assigned CASE A (see Fig. 6), which corresponds to solutions that do not represent any exchange of energy. At 117 s, a strong acceleration occurs, resulting in the search space definition associated with power assignment factors in the region defined by CASE G. This results in a dual source power supply to the vehicle, leading to the natural unloading of SCs, taking the SCs’ SoC value below the minimum threshold. In the next operations (cruising and deceleration or braking), verifying anSoC level of SCs below the selected minimum threshold, the strategy level guides the SA algorithm in the same way as in similar operations in previous periods. The decisions taken by SA are primarily driven by the long-term strategy level depending on the SoC values of the sources and the power demanded by the vehicle. In Fig. 5.3a, the graphical representation of the power assignment factors are displayed, depending on the search space restriction computed by the integrated rule-based SA approach.

Fig. 8 presents the ECE 15 drive cycle power sharing decomposition with an initial 100% SCs’ SoC. The full charged SCs assumption at the beginning of the driving cycle leads the strategy level to guide the SA algorithm differently from the previous simulation. Basically, the situations in which the strategy level directs the SA algorithm to different search spaces are related to power demand in standing, cruising and braking phases. In the first one, the strategy level reduces the search space to the region designated as CASE A in Fig. 8 (in the previous simulation it was CASE B, at the same time interval), due to the “right” energy level of the SCs to prepare the next operation (acceleration). In the cruising phases, the search space is reduced to the region

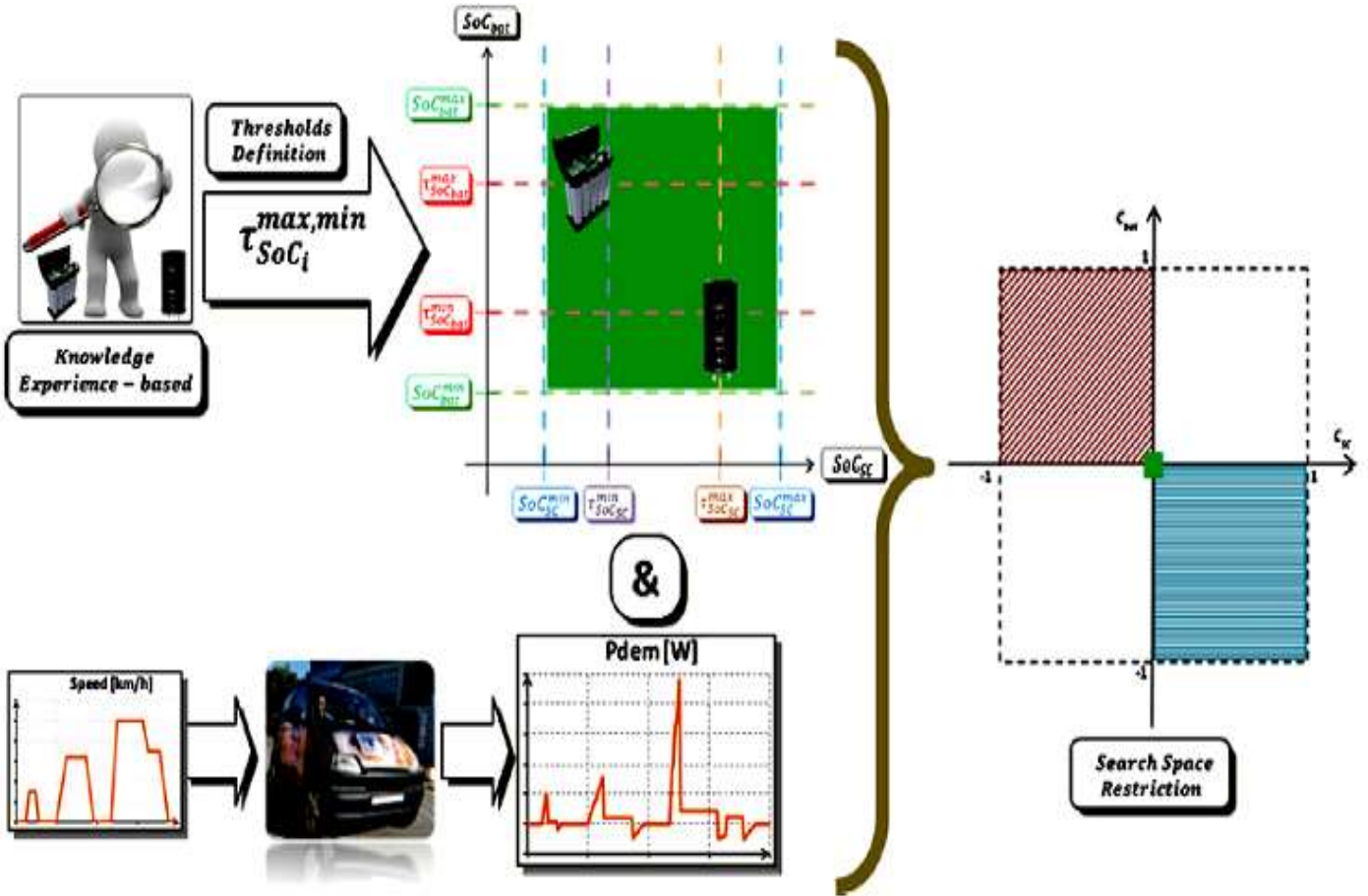
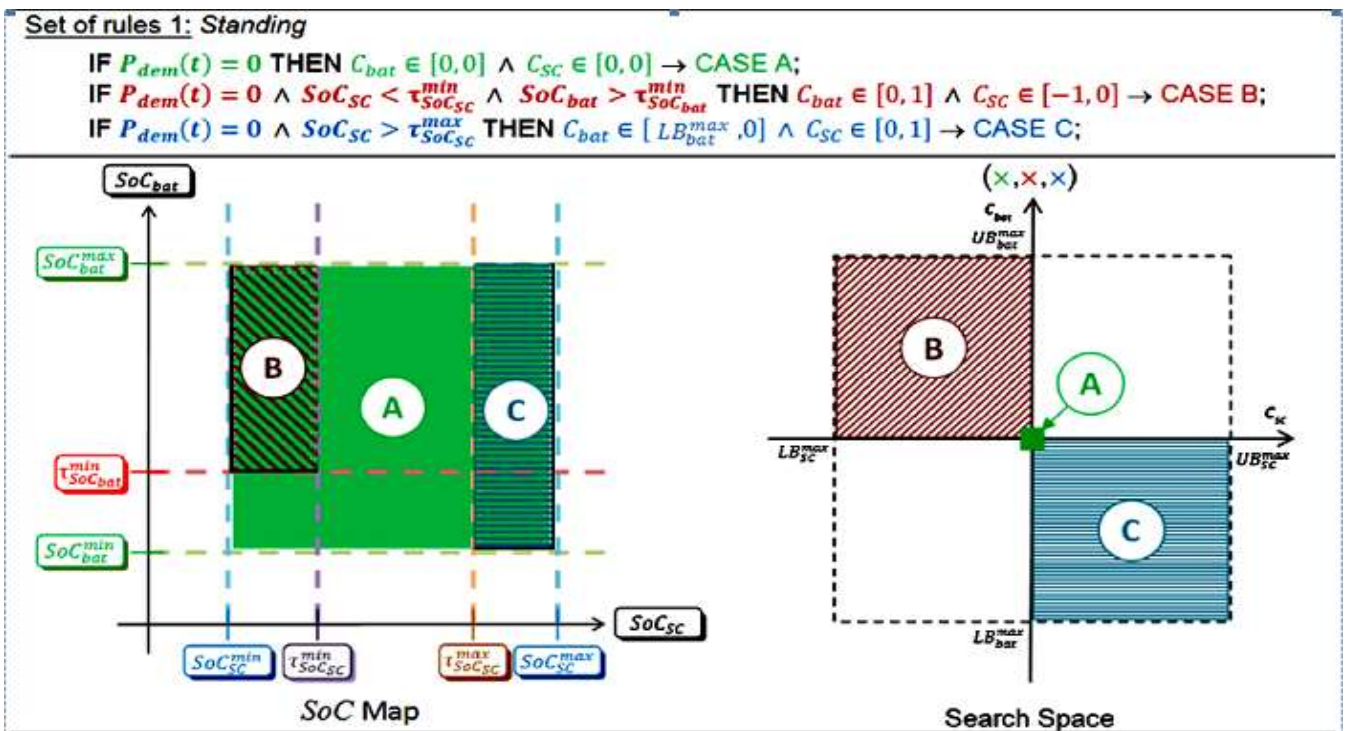


Fig 2. Search Space Restriction Process Based On Defined Soc Thresholds And Power Demand



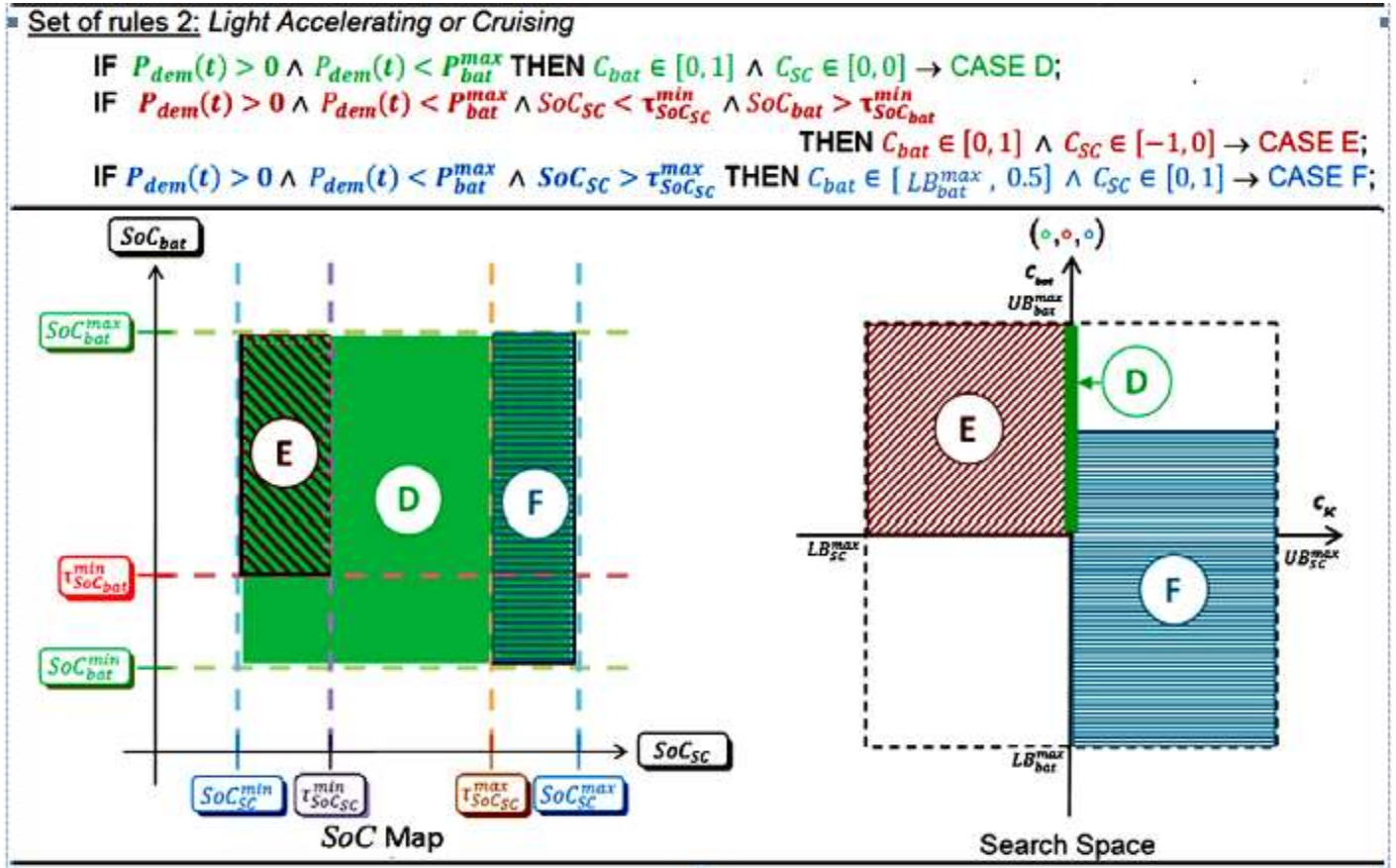
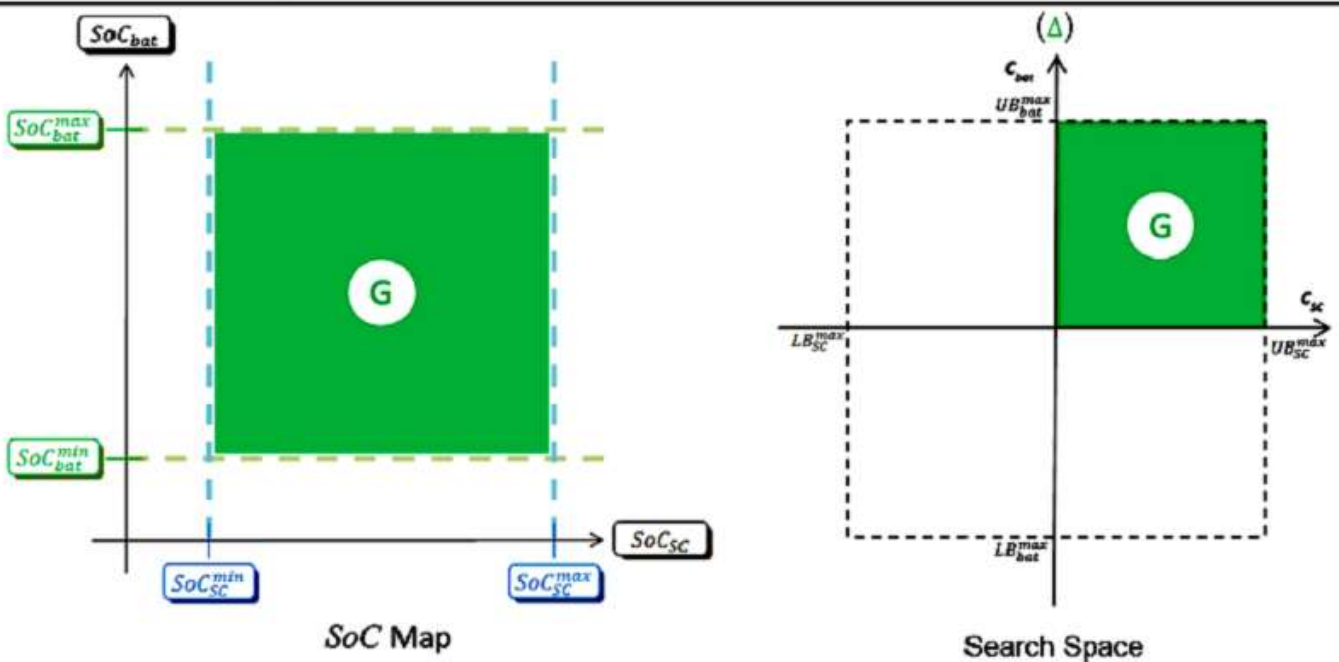


Fig 3.Weak-Rules for Long-Term Strategy Planning

Set of rules 3: High Acceleration

IF $P_{dem}(t) > P_{bat}^{max}$ THEN $C_{bat} \in [0, 1] \wedge C_{SC} \in [0, 1] \rightarrow$ CASE G;



Set of rules 4: Decelerating or Breaking

IF $P_{dem}(t) < 0$ THEN $C_{bat} \in [0, 0] \wedge C_{SC} \in [-1, 0] \rightarrow$ CASE H;

IF $P_{dem}(t) < 0 \wedge SoC_{SC} < \tau_{SoC_{SC}}^{min}$ THEN $C_{bat} \in [0, 1] \wedge C_{SC} \in [-1, 0] \rightarrow$ CASE I;

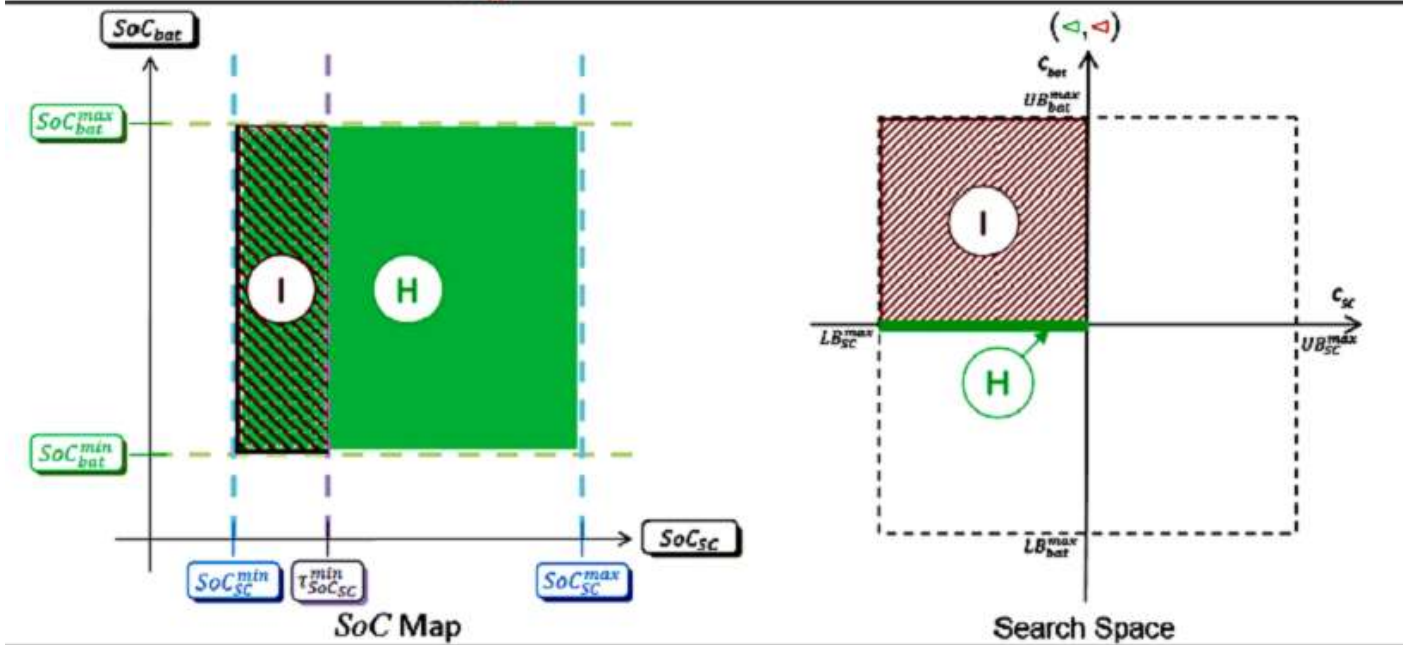


Fig 4. Medium-Rules for Long-Term Strategy Planning

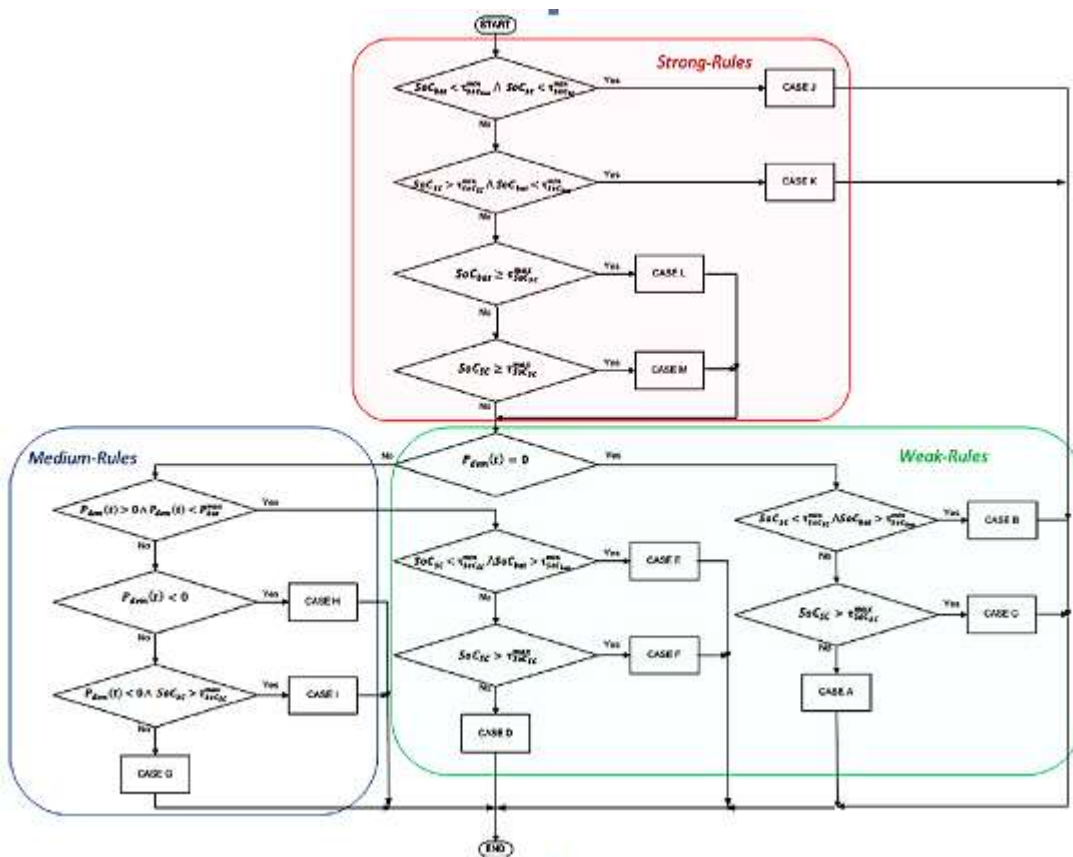


Fig 5. Flowchart of Dynamic Search Space Restriction Process

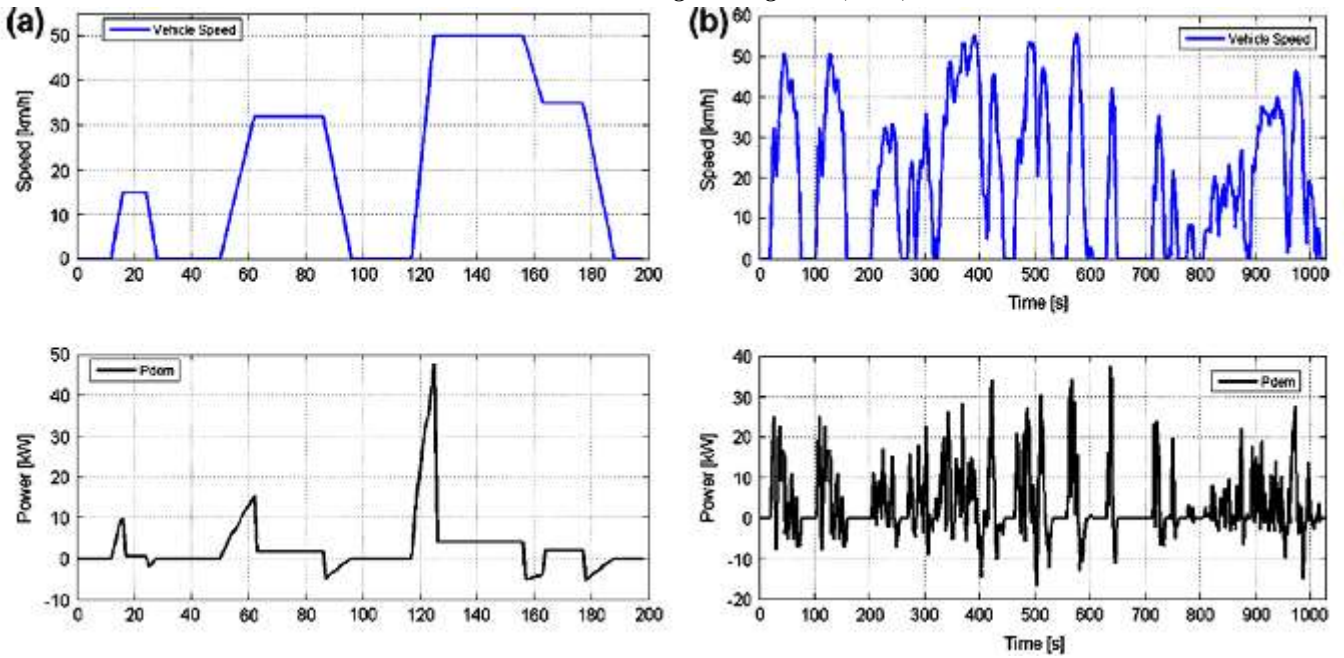


Fig 6. Speed And Veil Electrical Power Demand for: (A) Ece 15 Driving Cycle And (B) Artemis Low Motor Urban Total Driving Cycle

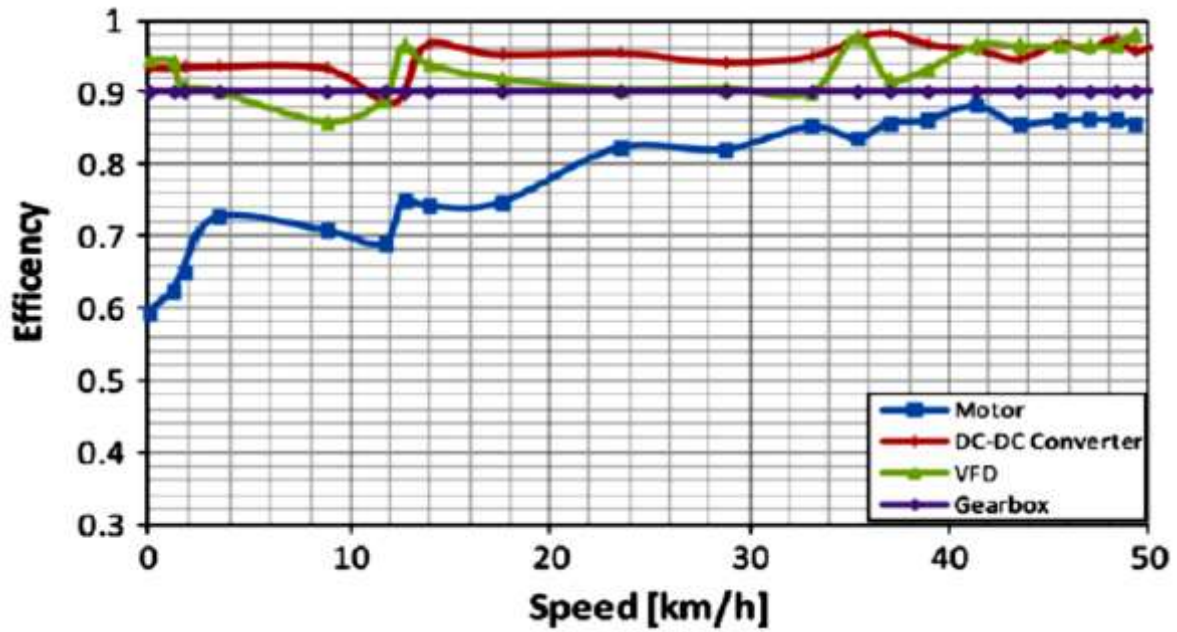


Fig 7. VEIL Powertrain Efficiencies (Electric Motor (H_m), Inverter (H_{vfd}) And Dc/Dconverter (H_{conv}))

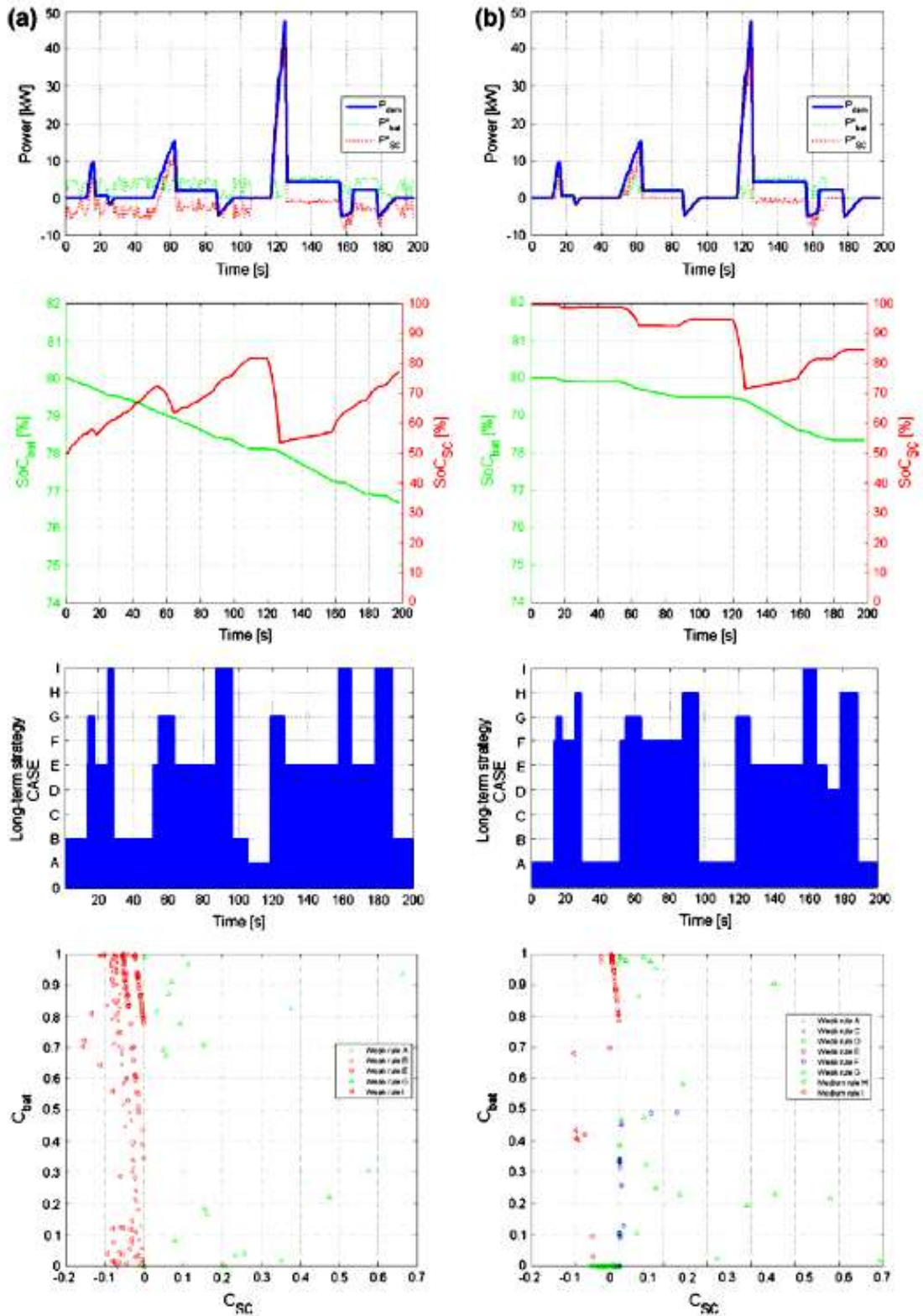


Fig 8. ECE 15 Driving Cycle Results For Different Scs' Beginning Soc Values: (A) Soc_{bat} = 80% And Soc_{sc} = 50% And (B) Soc_{bat} = 80% And Soc_{sc} = 100% (I – Sharing Power Results; ii– Socs Evolution; Iii – Long-Term Strategy Histogram; Iv – Power Assignment Factors).

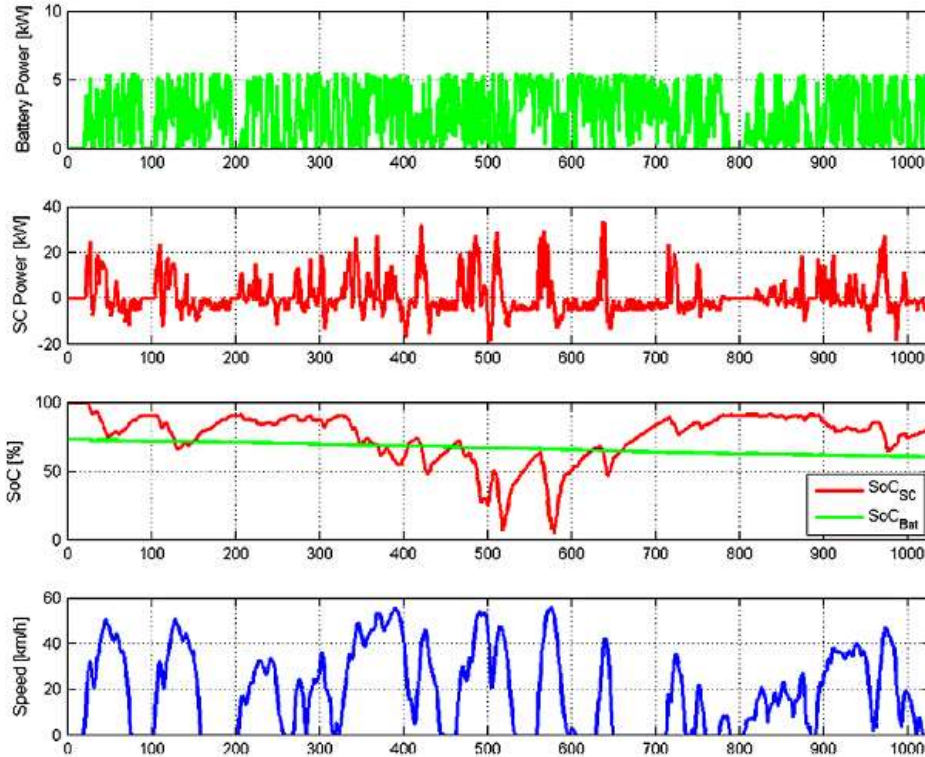


Fig 9.ARTEMIS Low Power Urban Driving Cycle Results.

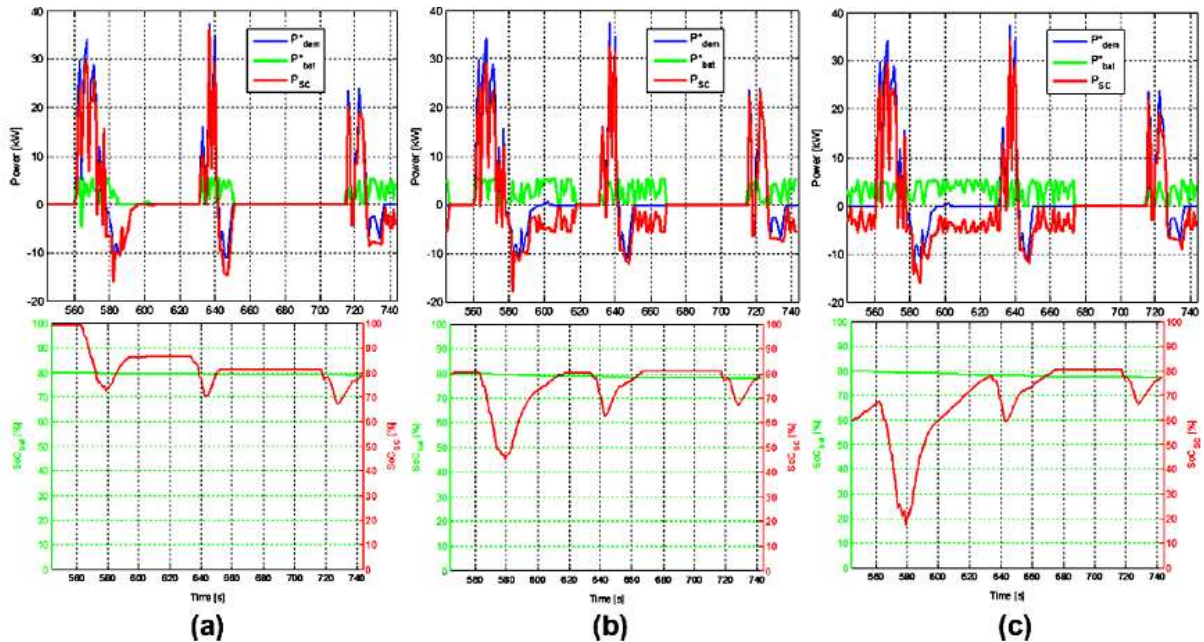


Fig 10. Part of ARTEMIS Low Power Urban Driving Cycle $T \in [544,744]$ S Results For Different Initial Scs' Soc: (A) 100%; (B) 80%; (C) 60%.

6. References

(1) Kahrobaeian and Y.-R. Mohamed, "Interactive distributed generation interface for flexible micro-grid operation in smart distribution systems," *IEEE Trans. Sustain. Energy*, vol. 3, no. 2, pp. 295–305, Apr. 2012.

(2) N. R. Tummuru, M. K. Mishra, and S. Srinivas, "Multifunctional VSC controlled microgrid using instantaneous symmetrical components theory," *IEEE Trans. Sustain. Energy*, vol. 5, no. 1, pp. 313–322, Jan. 2014.

(3) Y. Zhang, N. Gatsis, and G. Giannakis, "Robust energy management for microgrids with high-penetration renewables," *IEEE Trans. Sustain. Energy*, vol. 4, no. 4, pp. 944–953, Oct. 2013.

(4) R. Majumder, A. Ghosh, G. Ledwich, and F. Zare, "Load sharing and power quality enhanced operation of a distributed microgrid," *IET Renewable Power Gener.*, vol. 3, no. 2, pp. 109–119, Jun. 2009.

(5) J. Guerrero, P. C. Loh, T.-L. Lee, and M. Chandorkar, "Advanced control architectures for intelligent microgrids—Part II: Power quality, energy storage, and ac/dc microgrids," *IEEE Trans. Ind. Electron.*, vol. 60, no. 4, pp. 1263–1270, Dec. 2013.

(6) Y. Li, D. Vilathgamuwa, and P. C. Loh, "Microgrid power quality enhancement using a three-phase four-wire grid-interfacing compensator," *IEEE Trans. Ind. Appl.*, vol. 41, no. 6, pp. 1707–1719, Nov. 2005.

- (7) M. Schonardie, R. Coelho, R. Schweitzer, and D. Martins, "Control of the active and reactive power using dq0 transformation in a three-phase grid-connected PV system," in Proc. IEEE Int. Symp. Ind. Electron., May 2012, pp. 264–269.
- (8) R. S. Bajpai and R. Gupta, "Voltage and power flow control of grid connected wind generation system using DSTATCOM," in Proc. IEEE Power Energy Soc. Gen. Meeting—Convers. Del. Elect. Energy 21st Century, Jul. 2008, pp. 1–6.
- (9) M. Singh, V. Khadkikar, A. Chandra, and R. Varma, "Grid interconnection of renewable energy sources at the distribution level with power-quality improvement features," IEEE Trans. Power Del., vol. 26, no. 1, pp. 307–315, Jan. 2011.
- (10) H.-G. Yeh, D. Gayme, and S. Low, "Adaptive VAR control for distribution circuits with photovoltaic generators," IEEE Trans. Power Syst., vol. 27, no. 3, pp. 1656–1663, Aug. 2012.
- (11) Demoulias, "A new simple analytical method for calculating the optimum inverter size in grid-connected PV plants," Electr. Power Syst. Res., vol. 80, no. 10, pp. 1197–1204, 2010.
- (12) R. Tonkoski, D. Turcotte, and T. H. M. EL-Fouly, "Impact of high PV penetration on voltage profiles in residential neighborhoods," IEEE Trans. Sustain. Energy, vol. 3, no. 3, pp. 518–527, Jul. 2012.
- (13) X. Yu and A. Khambadkone, "Reliability analysis and cost optimization of parallel-inverter system," IEEE Trans. Ind. Electron., vol. 59, no. 10, pp. 3881–3889, Oct. 2012.
- (14) M. K. Mishra and K. Karthikeyan, "Design and analysis of voltage source inverter for active compensators to compensate unbalanced and nonlinear loads," in Proc. IEEE Int. Power Eng. Conf., 2007, pp. 649–654.
- (15) A. Ghosh and A. Joshi, "A new approach to load balancing and power factor correction in power distribution system," IEEE Trans. Power Del., vol. 15, no. 1, pp. 417–422, Jan. 2000.
- (16) U. Rao, M. K. Mishra, and A. Ghosh, "Control strategies for load compensation using instantaneous symmetrical component theory under different supply voltages," IEEE Trans. Power Del., vol. 23, no. 4,
- (17) P. Rodriguez et al., "A stationary reference frame grid synchronization system for three-phase grid-connected power converters under adverse grid conditions," IEEE Trans. Power Electron., vol. 27, no. 1, pp. 99–112, Jan. 2012.
- (18) S. Iyer, A. Ghosh, and A. Joshi, "Inverter topologies for DSTATCOM applications—A simulation study," Electr. Power Syst. Res., vol. 75, no. 23, pp. 161–170, 2005.
- (19) Y. Tang, P. C. Loh, P. Wang, F. H. Choo, and F. Gao, "Exploring inherent damping characteristic of LCL filters for three-phase grid-connected voltage source inverters," IEEE Trans. Power Electron., vol. 27, no. 3, pp. 1433–1443, Mar. 2012.
- (20) Vilathgamuwa, P. C. Loh, and Y. Li, "Protection of microgrids during utility voltage sags," IEEE Trans. Ind. Electron., vol. 53, no. 5, pp. 1427–1436, Oct. 2006.
- (21) M. Prodanovic and T. Green, "Control and filter design of three-phase inverters for high power quality grid connection," IEEE Trans. Power Electron., vol. 18, no. 1, pp. 373–380, Jan. 2003.
- (22) M. Hamid, A. Jusoh, and M. Anwari, "Photovoltaic plant with reduced output current harmonics using generation-side active power conditioner," IET Renewable Power Gener., vol. 8, no. 7, pp. 817–826, Sep. 2014.
- (23) L. Rolim, D. da Costa, and M. Aredes, "Analysis and software implementation of a robust synchronizing PLL circuit based on the pq theory," IEEE Trans. Ind. Electron., vol. 53, no. 6, pp. 1919–1926, Dec. 2006.
- (24) L. Shiguo, "Optimal design of dc voltage close loop control for an active power filter," in Proc. IEEE Int. Conf. Power Electron. Drive Syst., Feb. 1995, pp. 565–570.